PAPER

Highly luminescent dual mode rare-earth nanorod assisted multi-stage excitable security ink for anti-counterfeiting applications†

Pawan Kumar, Jaya Dwivedi and Bipin Kumar Gupta*

In this paper, the synthesis of multi-stage excitable (379 nm, 980 nm and 1550 nm), highly luminescent Y_2O_3:Yb^{3+}/Er^{3+} nanorods by a hydrothermal method which can emit both hypersensitive green (562 nm) and strong red (660 nm) in a single host lattice and which can be used for a transparent security ink application is reported. Furthermore, these luminescent nanorods also exhibit both down-shift (1127 nm) as well as upconversion (562 nm) features at a single excitation near infrared wavelength of 980 nm. The characterization of these luminescent nanorods was explored by studying their structure/microstructure, using photoluminescence and time-resolved spectroscopic techniques. Furthermore, these luminescent nanorods exhibited the tuning of emission colours from red to green by controlling the sintering temperature. It was demonstrated that these novel luminescent nanorods offer new opportunities for making high-end, multi-stage excitable transparent security ink. The state-of-art production process of ink is easy and it is most suitable for bulk production at an economical cost. Thus, the security inks could be used globally in applications for protection against counterfeiting.

Introduction

Recently, data security has become an important issue for each sector of industry as well as in the government offices in the contemporary world. The increasing trend of counterfeiting has become more common in all walks of life and it is causing significant damage and as well as posing serious security threats to individuals, companies, and the nation as a whole. The counterfeiting of currency has a detrimental effect on socio-economic processes of a society, which leads to reduction in the value of currency. Counterfeiting in the medical sector can severely jeopardize human health, whereas counterfeiting of documents is infringement of copyright laws. Consequently, governments and private industries all over the world have to bear a loss of billions of dollars annually because of illegal counterfeiting activities.[1–5] Currently, one of the major issues is to completely check the counterfeiting of currency as well as important documents including those related to strategic sectors of any nation. During the last decade, millions of dollars have been spent worldwide by governments and industries to safeguard their products and currencies from being counterfeited and the efforts have yielded positive results. Almost, every country has opted for protection against fake currencies by either use of holographic techniques or by use of visible luminescent ink or bands and so on (which glow under ultraviolet (UV) light).[6–10] Furthermore, commercial and industrial sectors, particularly those producing branded goods and pharmaceuticals, have also adopted these techniques and have benefitted tremendously from these safety measures against counterfeiting.[11,12] Besides this, another area of security where a more overt colorimetric indicator can be used is food security, where sensing the presence of oxygen is a principal goal – the area of intelligent packaging.[13]

During the past decades, a number of anti-counterfeiting technologies such as simple markers, plasmonic security labels, holograms, security inks and so on, were developed as a shield against counterfeiting.[10,14] Today, the development of new materials for anti-counterfeiting is of great importance for their use in protection and detection of counterfeiting. However, from the security point of view, the luminescent materials provide improved security because of their unique physical, chemical and optical properties. Although there are many semiconductor nanoparticles such as cadmium sulfide, cadmium selenide, cadmium telluride and so on, which have been reported to be used as luminescent security ink, they have their own disadvantages such as toxicity, broad emission bands and solubility in harmful solvents. The formation of a stable and transparent solution of these nanoparticles is also difficult. Furthermore, the lanthanide doped phosphors have many advantages over these materials such as low toxicity, sharp emission bands and solubility. Therefore, the lanthanide-based

Luminescent Materials and Devices Group, Materials Physics and Engineering Division, CSIR-National Physical Laboratory, Dr K. S. Krishnan Road, New Delhi-110012, India. E-mail: bipinbhu@yahoo.com; Fax: +91-11-45609310; Tel: +91-11-45609385

transparent security ink has become a successful tool for security labels, identification markers and barcode systems.

Our earlier efforts were to develop red emitting down-shift invisible security ink based on polyvinyl alcohol (PVA) as well as sodium hexametaphosphate (SHMP) medium and these were used successfully to demonstrate their use in terms of security coding.[2] Efforts are being made by several groups to develop either upconversion or downconversion security ink based on lanthanide materials.[4,5] Only a single stage coding capability has been achieved so far by using these luminescent materials. This implies that the luminescent fluorophores developed can be excited by a single wavelength, which subsequently emits only at a single wavelength. This coding technique appears to be comparatively less effective at protecting documents. Because of this reason, a high performance, multi-stage coding with many excitations and at least two colour emissions has been awaited for a long time. To develop a phosphor with all the desirable properties at an economical cost is a great challenge in this area which is being addressed in the present investigations. Now in the present research, our purpose was to develop a transparent security ink with multi-stage coding in a single host based on a highly luminescent nanostructure which is not only economic but also beneficial for high end protection. Earlier, several attempts had been made but their protection techniques were common and utilized single stage protection. Even nowadays, many groups are trying to use the dual mode emission by incorporating two or more kinds of activator in a single host, although their intention was entirely different, because incorporating many activators is an expensive technique and dispersion is also an important issue.[15] A single host lattice based luminescent material with single activator which can emit both upconversion as well as down-shift simultaneously has been developed in the current research. As a result, it provides multi-stage coding in a host. Furthermore, the choice of the material for security ink applications depends upon the physical and chemical properties as well as the morphology of nanomaterials. The yttrium oxide (Y_2O_3) is an attractive host for security ink applications because of its physical, chemical and optical properties. An additional advantage of using nanorods is that it also helps to bring down the amount of material required for their use in security ink applications, thus reducing the production cost and as well the rod shape is good in fillers in a cellulose ink matrix.[16] On the basis of this concept, highly luminescent nanorod-based, multi-stage excitable and transparent inks for security applications were developed.

In this study, the development of multi-stage excitable (379 nm, 980 nm and 1550 nm), highly luminescent Y_2O_3:Yb^{3+}/Er^{3+} nanorods was demonstrated by using a hydrothermal technique for security inks, which can intensely emit hypersensitive green and strong red colours. Furthermore, these nanorods have also shown both down-shift as well as having an upconversion nature for a single excitation wavelength at 980 nm which has been reported for such applications. The gross structural, morphological, and microstructural investigations of these luminescent nanorods have been carried out through X-ray diffraction, scanning electron microscopy and high-resolution transmission electron microscopy/transmission electron microscopy techniques. The spectroscopic characterizations of these luminescent nanorods have been done through photoluminescence and time-resolved spectroscopic techniques. The promising use of this luminescent nanorod-based transparent security ink for security codes on black paper using a standard screen printing technique as well as security spot marking on currency for a high end protection application which exhibits a new paradigm shift in luminescent security ink applications was also demonstrated.

Experimental section

The precursors: Y_2O_3 (99.99%), erbium nitrate pentahydrate ($Er(NO_3)_3 \cdot 5H_2O$, 99.99%), ytterbium(III) chloride hexahydrate ($YbCl_3 \cdot 6H_2O$, 99.99%) and N-cetyl-N,N,N trimethylammonium bromide ($C_{19}H_{42}BrN$, CTAB) were purchased from Sigma-Aldrich. All reagents were of analytical (AR) grade and used as received without further purification. Double distilled water was used throughout the experiments.

The Y_2O_3:Yb^{3+}/Er^{3+} nanorods were synthesized using a hydrothermal method. The precursors used were: Y_2O_3, $Er(NO_3)_3 \cdot 5H_2O$, $YbCl_3 \cdot 6H_2O$ and CTAB. The nanorods were doped with an optimized concentration of rare earth ions (1 mol% of Er and 2 mol% of Yb). The stoichiometric amount of Y_2O_3 was dissolved in nitric acid followed by stirring at 80 °C until the solution turned into a transparent nitrate solution. The precursors $Er(NO_3)_3 \cdot 5H_2O$, $YbCl_3 \cdot 6H_2O$ and CTAB were dissolved in deionized water. The prepared solutions were mixed in ethanol solution (1 : 5 ethanol : water) under vigorous stirring at room temperature. The sodium hydroxide solution was added to the above mixture and then stirred magnetically until the pH of the final solution became ~12. Several runs were made using different pH values and ultimately, it was found that a pH of ~12 favoured the reaction which produced long uniform nanorods. Then this solution was transferred into a sealed hydrothermal bomb which was kept at 185 °C for 10 hours in a box furnace. The precipitate obtained was centrifuged several times with de-ionized water at 5000 rpm and then dried at 100 °C. The final product was heated at 1000 °C in a box furnace for 6 hours. In this method, the yield of material was more than 90% with a high degree of homogeneity throughout the sample.

A standard polyvinyl chloride (PVC) gold medium (locally fabricated, printing ink manufactured by Commercial Techno Colours, Ram Nagar, Varanasi 221005, India) was used to disperse the as-synthesized dual mode Y_2O_3:Yb^{3+}/Er^{3+} nanorods before use as security printing application. The commercial PVC gold medium used in the present investigation is shown in Fig. S1 (see ESI†). The choice of dispersive medium is important for two purposes, firstly to disperse rare earth metals into the medium without formation of clusters or agglomerates of nanorods and secondly, for obtaining better printing, the viscosity of the medium (3000 μP) is very important as it provides the sticky nature of the printing paper. Our earlier efforts using PVA as medium failed to avoid the formation of clusters.[2] In a typical experiment, 50 mL of PVC gold medium solution was placed in a beaker and 200 mg of Y_2O_3:Yb^{3+}/Er^{3+}

This journal is © The Royal Society of Chemistry 2014

J. Mater. Chem. C, 2014, **2**, 10468–10475 | **10469**

nanorods were mixed with the solution. The resultant mixture was mixed ultrasonically at 45 kHz for 30 min to obtain a good dispersion. The highly transparent (~81%) colloidal solution was obtained which is shown in Fig. S2 (see ESI†). To make a pattern onto black paper, a standard screen printing technique for object printing as well as for alphabets was used.

The gross crystal structure analysis of the samples was carried by using X-ray powder diffraction (XRD) with a Bruker AXS D8 Advance X-ray diffractometer, using Cu Kα_1 radiation ($\lambda = 1.5406$ Å). The UV absorption spectra were recorded using a Shimadzu UV 160 UV-visible spectrometer. Thermogravimetric analysis was done using a thermal analysis instrument with a heating rate of 10 °C min^{-1} in an air flow of 100 mL min^{-1}. Raman studies were carried out using a Renishaw inVia Raman spectrometer, with an excitation source of 785 nm. The surface morphology and energy dispersive X-ray (EDAX) was examined using a Carl ZEISS EVO 18 scanning electron microscope with 10 kV operating voltage. Transmission electron microscopy (TEM) and high-resolution transmission microscopy (HRTEM) micrographs were recorded using a Tecnai G2 S-Twin scanning transmission electron microscope with a field emission gun operating at 300 kV. The photoluminescence (PL) and time-resolved spectroscopy were carried out using an Edinburgh Instruments spectrometer, where a xenon lamp acts as the source of excitation. The PL mapping of luminescent nanorods was performed using a WITech alpha 300R+ confocal PL microscope system, where 375, 980 and 1550 nm diode lasers act as a source of excitation. The near infrared (NIR) emissions above 1100 nm were recorded using a NIR detector. The fluorescent images were recorded using a Nikon ECLIPSE 80i microscope.

Results and discussion

A novel strategy was adopted to synthesize highly luminescent Y_2O_3:Yb^{3+}/Er^{3+} nanorods using a customized hydrothermal method. The proper interaction between the dopant (Yb^{3+}) and co-dopant (Er^{3+}) is very important to obtain highly efficient luminescent materials. Here, the optimization of the concentration played a key role in getting bright PL material. The addition of the Yb^{3+} ion increases the absorption because the Yb^{3+} ion efficiently absorbs the energy and becomes excited. The excited Yb^{3+} ion transfers this energy to the Er^{3+} ion which promotes its own electrons in a higher energy level as shown in Fig. S3 (see ESI†). Subsequently, the population in the excited states of the Er^{3+} increases significantly. The energy transfer depends upon the doping concentration of both dopant as well as co-dopant. The main focus of the present investigation is to optimize the green PL emission intensity of Y_2O_3:Yb^{3+}/Er^{3+} nanorods while keeping the concentration of Yb^{3+} fixed. The PL intensity of the green emission was varied with respect to the change in concentration of Er^{3+} from 0.5 to 2.5 mol% at a fixed concentration of Yb^{3+} (2 mol%) (see Fig. S4 in the ESI†). The optimum concentration of Er^{3+} was shown to be ~1 mol%. Furthermore, the optimum concentration of Yb^{3+} was also investigated from 1–3 mol% at a fixed optimum concentration of Er^{3+} of ~1 mol%. It was found that the efficient energy

transfer with high green emission was obtained at 2 mol% as shown in Fig. S5 (see ESI†). Thus, the optimum concentrations of dopant and co-dopant were obtained: Yb^{3+} ~2 mol%, Er^{3+} ~1 mol% for Y_2O_3:Yb^{3+}/Er^{3+} nanorods. The same optimum concentration of the sample also exhibits unique features in terms of downshift with a strong green emission at 562 nm upon excitation at 379 nm. Furthermore, the energy level diagram of the optimum sample for the down-shift is shown in Fig. S6 (see ESI†). Furthermore, luminescent nanorods synthesized at the optimum concentration were fully characterized using several structural/microstructural and spectroscopic techniques.

The crystalline structure of Y_2O_3:Yb^{3+}/Er^{3+} nanorods were investigated using X-ray powder diffraction (CuKα_1, $\lambda = 1.5406$ Å). Fig. 1a shows the XRD pattern of Y_2O_3:Yb^{3+}/Er^{3+} nanorods heat treated at 1000 °C. The XRD results show that nanorods have a cubic phase with good crystallinity (JCPDS card no. 43-1036). The estimated lattice parameters for Y_2O_3:Yb^{3+}/Er^{3+} nanorods were $a = b = c = (10.5869 \pm 0.0043)$ Å which are comparable to standard lattice parameters $a = b = c = 10.6040$ Å. The inset of Fig. 1a shows the proposed crystal structure of Y_2O_3 where Y atoms are replaced by Er and Yb atoms. Fig. 1b represents the Raman spectrum of luminescent nanorods. The Raman spectrum reveals that the host lattice has bands at 377 cm^{-1}, 428 cm^{-1}, 465 cm^{-1}, 511 cm^{-1} and 541 cm^{-1}. The band present at 377 cm^{-1} represents the cubic phase of Y_2O_3:Yb^{3+}/Er^{3+} nanorods. The results obtained are in good agreement with the earlier reports for the Raman spectrum of the Y_2O_3 host.[17] Fig. 1c demonstrates the Fourier-transform infrared (FT-IR) spectrum of nanorods sintered at 1000 °C as well as the as-synthesized nanorods at 185 °C.

The FT-IR spectrum of the nanorods heated at 1000 °C shows no peak around 3400 cm^{-1} because of the absence of the OH

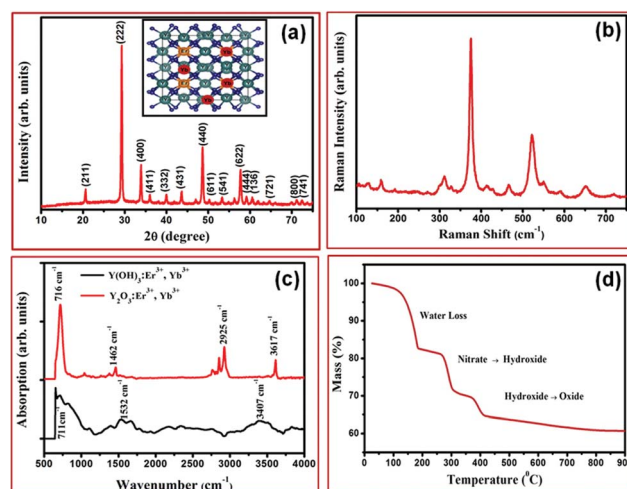Fig. 1 (a) XRD pattern of Y_2O_3:Yb^{3+}/Er^{3+} nanorods treated at 1000 °C. The right inset shows the proposed model of the cubic cell of the structure of Y_2O_3:Yb^{3+}/Er^{3+} nanorods, (b) shows the Raman spectrum of Y_2O_3:Yb^{3+}/Er^{3+} nanorods, (c) the FT-IR spectrum of Y_2O_3:Yb^{3+}/Er^{3+} nanorods and (d) results of the thermogravimetric analysis (TGA) of Y_2O_3:Yb^{3+}/Er^{3+} nanorods.

group, which suggests that the hydroxide formed $(Y(OH)_3\text{-}Yb^{3+}/Er^{3+})$ at 185 °C during the hydrothermal process is completely converted into the oxide form $(Y_2O_3\text{:}Yb^{3+}/Er^{3+})$ on sintering at 1000 °C.

It is well known that the surface to volume ratio of the nanorod is larger than the spherical particle. The rare earth ions near the surface have large numbers of unsaturated bonds, which ultimately lead to surface defects and reaction with OH-groups. Consequently, the luminescence intensity of the as-synthesized nanorods is lower than that of the heat treated nanorods. This indicates that the luminescence increases because of the absence of the OH group in the $Y_2O_3\text{:}Yb^{3+}/Er^{3+}$ nanorods.[18] To understand the thermal decomposition of as-synthesized $Y_2O_3\text{:}Yb^{3+}/Er^{3+}$ nanorods, the TGA investigation was carried out. Fig. 1d exhibits the TGA analysis of $Y_2O_3\text{:}Yb^{3+}/Er^{3+}$ nanorods, which demonstrates that the three temperature intervals corresponded to three substantial weight loss processes. The first interlude between 100–182 °C corresponds to water loss. The interlude between 270–310 °C is because of the decomposition of nitrates into hydroxides. The last interlude between 370 °C and 410 °C is because of the decomposition of hydroxide into oxide. The results obtained are consistent with results reported earlier.[19]

The surface morphology was examined by using SEM. Fig. 2a demonstrates the SEM image of nanorods. The image shows that the synthesized nanorods have a highly dense nano-structure with a uniform size distribution. The magnified version of the SEM image of the nanorods is shown in Fig. 2b which clearly demonstrates the dimensions of the nanorods which are in the range of nanometers: 50–90 nm diameter and length ~1–3 μm at optimum growth conditions (1000 °C for 6 hours). The morphology of these luminescent materials

originates as rod shapes because of the initial nucleation of the hexa-hydroxy phase formation during the intermediate reaction (after the hydrothermal process and before the final sintering at 1000 °C for oxide phase formation) where a nitrate solution of metals are converted into the hydroxy phase at 185 °C as shown in Fig. S7 (see ESI†). The surface morphologies of $Y_2O_3\text{:}Yb^{3+}/Er^{3+}$ nanorods at different time intervals during the growth at 1000 °C and statistical histogram of size distribution are shown in Fig. S8 and S9 (for more details, see the ESI†). The different growth temperatures were employed to optimize the lumines-cence behaviour as well as the controlled morphologies. The EDAX analysis was performed for the element detection. Fig. 2c demonstrates the elemental analysis of nanorods, which confirmed the presence of Er, O, Y and Yb elements. The microstructural analysis of the synthesized nanorods was done using TEM. Fig. 2d shows the typical TEM micrograph of the nanorods. The TEM micrograph of an individual nanorod is shown in Fig. 2e. A typical HRTEM micrograph of a nanorod is shown in Fig. 2f and shows that the nanorods have well resolved lattice fringes without distortion which shows the good quality of the crystal. The estimated d-spacing of the nanorods is ~0.302 nm which is comparable to the 0.306 nm corresponding to the (222) plane (JCPDS card no. 43-1036).

The PL and time-resolved spectroscopy were carried out to explore the spectroscopic features of the luminescent nanorods which legitimize its potential use for high-end security ink applications. The emission spectrum of $Y_2O_3\text{:}Yb^{3+}/Er^{3+}$ nano-rods at 980 nm excitation is shown in Fig. 3a. The emission spectrum demonstrates that there are two emission bands: one band having a peak at 562 nm (green emission) and another at 660 nm (red emission). The green band corresponds to $^2H_{11/2}$, $^4S_{3/2} \rightarrow {}^4I_{15/2}$ transition whereas the red emission band is a

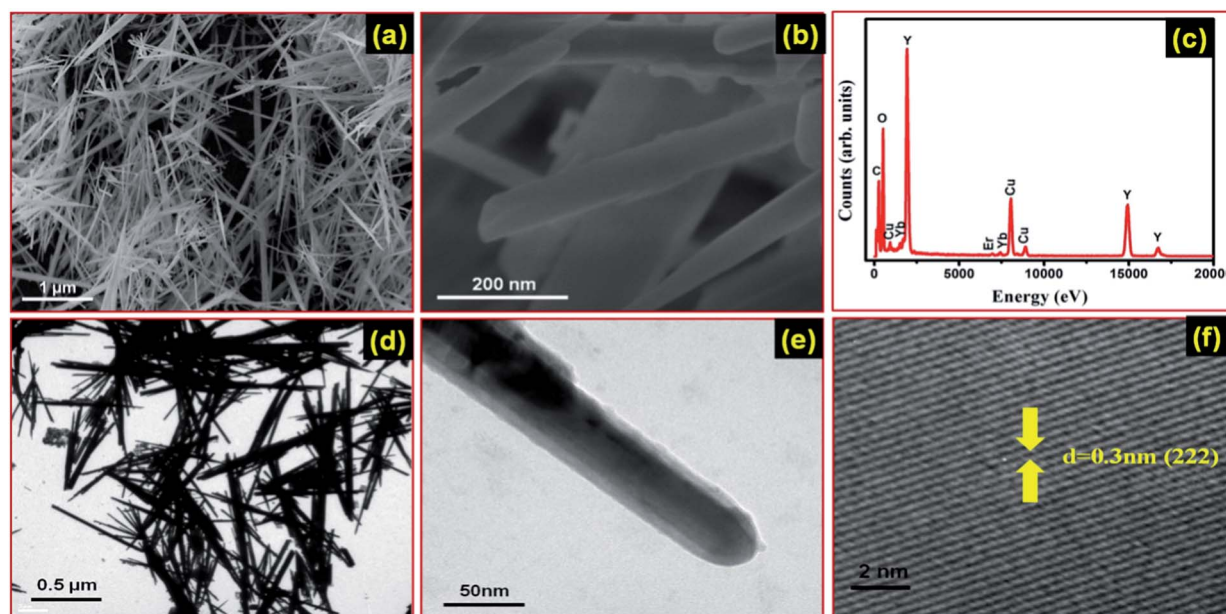**Fig. 2** (a) and (b) show the scanning electron microscopy (SEM) images of $Y_2O_3\text{:}Yb^{3+}/Er^{3+}$ nanorods and a magnified view of (a) respectively, (c) shows the results of the EDAX analysis of the $Y_2O_3\text{:}Yb^{3+}/Er^{3+}$ nanorods, (d) and (e) show the typical TEM image of nanorods and single nanorod, respectively, and (f) HRTEM results of $Y_2O_3\text{:}Yb^{3+}/Er^{3+}$ nanorod.
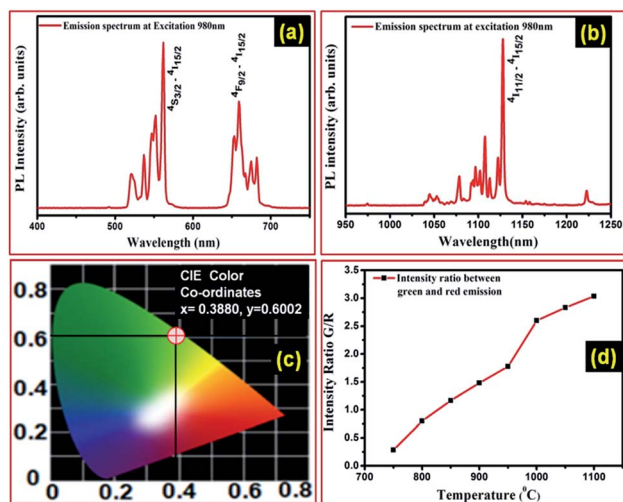
This journal is © The Royal Society of Chemistry 2014

J. Mater. Chem. C, 2014, **2**, 10468–10475 | **10471**

Fig. 3 (a) and (b) show the PL emission spectra of Y_2O_3:Yb^{3+}/Er^{3+} nanorods at an excitation of 980 nm, (c) demonstrates the CIE colour coordinates of green emission and (d) shows the ratio between green and red emission (I_G/I_R) with temperature.

Fig. 4 (a) shows the PL emission spectrum (460–730 nm visible region) of Y_2O_3:Yb^{3+}/Er^{3+} nanorods at an excitation of 1550 nm. (b) Represents the CIE colour coordinates of green emission of Y_2O_3:Yb^{3+}/Er^{3+} nanorods at an excitation of 1550 nm in the visible region, (c) exhibits the PL emission spectrum of Y_2O_3:Yb^{3+}/Er^{3+} nanorods at an excitation of 1550 nm in the NIR region (750–1050 nm), (d) shows the excitation spectrum of Y_2O_3:Yb^{3+}/Er^{3+} nanorods at an emission of 562 nm and (e) an emission spectrum of Y_2O_3:Yb^{3+}/Er^{3+} nanorods at an excitation of 379 nm and (f) shows the CIE colour coordinates.

consequence of $^4F_{9/2} \rightarrow {}^4I_{15/2}$ transition. The emission intensity of the green emission is greater than the red emission. The upconversion in Y_2O_3:Yb^{3+}/Er^{3+} nanorods can be explained by two mechanisms, energy transfer and excited state absorption (ESA).[20–22] The Yb^{3+} ions absorb the laser photons and transfer this energy to the Er^{3+} ion and because of this the population at $^4I_{11/2}$ increases. The populated $^4I_{11/2}$ level is further excited by three processes: ESA, energy transfer from the neighbouring Er^{3+} ion and energy transfer from the Yb^{3+} ion. The excited $^4F_{7/2}$ level usually relaxes non-radiatively to two lower energy levels: $^2H_{11/2}$ and $^4S_{3/2}$. The radiative emission from $^2H_{11/2}$ and $^4S_{3/2}$ energy levels to the ground state $^4I_{15/2}$ produces the green emission. The populated $^4F_{7/2}$ level also relaxes non-radiatively to $^4I_{13/2}$. The $^4I_{13/2}$ level is excited to the $^4F_{9/2}$ level by the same mechanism as described previously. The $^4F_{9/2}$ level relaxes radiatively which causes red emission. Fig. 3b demonstrates the emission spectra at excitation at 980 nm in the NIR region. This result demonstrates that the Y_2O_3:Yb^{3+}/Er^{3+} nanorods have a strong emission peak at 1127 nm, corresponding to excitation at 980 nm which has not so far been reported in the literature. An additional, interesting feature of the Y_2O_3:Yb^{3+}/Er^{3+} nanorods is shown in Fig. S10 (see ESI†), where the emission spectrum exhibits the downshift characteristic of Y_2O_3:Yb^{3+}/Er^{3+} nanorods in the NIR range of 1300–1700 nm at 980 nm excitation wavelength which has not so far been reported for this system. Fig. 3c shows the International Commission on Illumination (CIE) colour coordinates corresponding to emission at 980 nm with values of $x = 0.3880$ and $y = 0.6002$. The tuning of the emission wavelength from red to green is shown in Fig. 3d. Fig. 3d shows the intensity ratio of green to red emission (I_G/I_R) at different temperatures. The green colour intensity is enhanced with increase in temperature leading to an increase in the intensity ratio.

Fig. 4a demonstrates the emission spectrum of nanorods having strong green emission at 564 nm which corresponds to
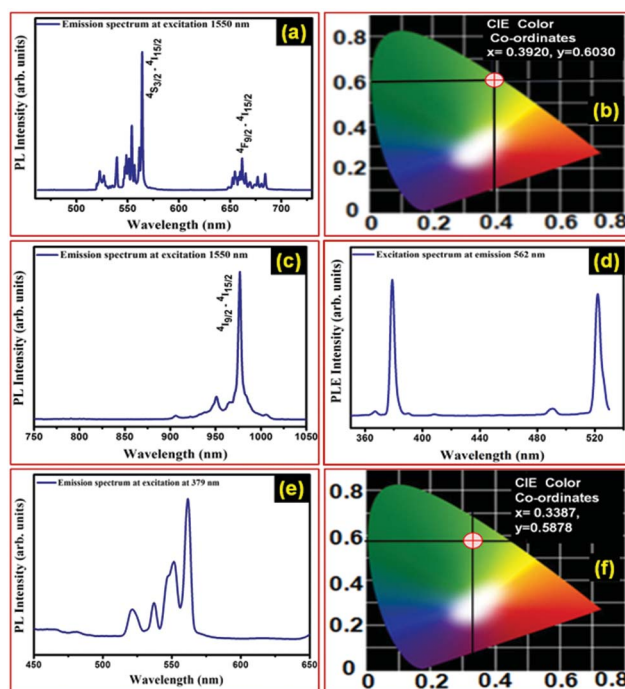
an excitation wavelength at 1550 nm which has not so far been reported in the literature. Fig. 4b shows the corresponding CIE colour coordinates with values of $x = 0.3920$ and $y = 0.6030$. This emission provides additional high-end security in the visible range which has not been reported before for security ink applications.[4,5] Fig. 4c exhibits the emission spectrum at excitation of 1550 nm in NIR region. The result demonstrates that the Y_2O_3:Yb^{3+}/Er^{3+} nanorods have a strong emission peak at 976 nm which corresponds to excitation at 1550 nm. The upconversion behavior of Y_2O_3:Yb^{3+}/Er^{3+} nanorods at an excitation wavelength of 1550 nm is shown in Fig. S11 (see ESI†). Fig. 4d shows the excitation spectrum at an emission of 562 nm. The emission of Y_2O_3:Yb^{3+}/Er^{3+} nanorods at an excitation of 379 nm is shown in Fig. 4e, where a strong green emission can be easily seen which is required for the purposes of this security ink application. Fig. 4f demonstrates the CIE colour coordinates with values $x = 0.3387$ and $y = 0.5878$. Fig. S12 and S13 (see ESI†) show the emission spectra of Y_2O_3:Yb^{3+}/Er^{3+}nanorods at excitation wavelengths of 488 and 522 nm which could also be utilized for the proposed application.

Furthermore, uniform emission from the Y_2O_3:Yb^{3+}/Er^{3+} luminescent nanorod was examined by a fluorescent microscopic technique (Nikon ECLIPSE 80i microscope). Fig. 5a and b clearly show a high contrast, hypersensitive green and red
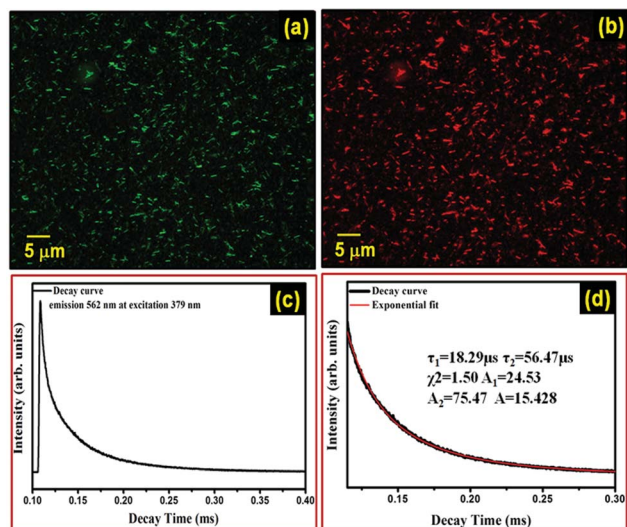
Fig. 5 (a) and (b) show the fluorescent images of Y_2O_3:Yb^{3+}/Er^{3+} nanorods corresponding to the excitation wavelength of 375 nm and 980 nm, respectively, (c) TRPL decay profile of Y_2O_3:Yb^{3+}/Er^{3+} nanorods recorded at room temperature while monitoring the emission at 562 nm, at an excitation wavelength of 379 nm and (d) exponential fitting of the decay profile which gives life time data and the parameters generated by the exponential fitting.

fluorescent image of Y_2O_3:Yb^{3+}/Er^{3+} nanorods at excitation wavelengths of 375 nm and 980 nm (externally equipped diode lasers compatible with the Nikon ECLIPSE 80i microscope) without auto-fluorescence from the background. The fluorescent images obtained reveal that these nanorods exhibit the uniform spatial distribution of red and green colours from different points of the nanorods.

The time-resolved photoluminescence (TRPL) was recorded using a single photon counting technique with a microsecond xenon flash lamp as the source of the excitation. The decay life time is an important parameter for determining the performance of a luminescent material and its suitable potential applications.[24,25] The efficiency of the radiative recombination depends on the decay time of the particular transition of the activator.[25] The luminescence decay profile as well as the exponential fitting of the results obtained are shown in Fig. 5c and d. Fig. 5c exhibits the decay profile of Y_2O_3:Yb^{3+}/Er^{3+} nanorods corresponding to excitation at 379 nm with emission of 562 nm. The life time data obtained from the luminescent nanorods was best fitted to a double-exponential function as,

$$I(t) = A_1 \exp(-t/\tau_1) + A_2 \exp(-t/\tau_2) \qquad (1)$$

where τ_1 and τ_2 are the decay life times of the luminescence, and A_1 and A_2 are the weighting parameters. Fig. 5d demonstrates the exponential fitting of decay profile as described in eqn (1). The parameters generated from fitting are listed in the inset in Fig. 5d. The observed life times are $\tau_1 \sim 18.29$ μs and $\tau_2 \sim 56.47$ μs. For double exponential decay, the average life time, τ_{av} is usually tailored to substitute the various components of the

luminescence life time, which is determined by the following equation:[23,24]

$$\tau_{av} = (A_1\tau_1{}^2 + A_2\tau_2{}^2)/(A_1\tau_1 + A_2\tau_2) \qquad (2)$$

The average life time of Y_2O_3:Yb^{3+}/Er^{3+} nanorods is calculated as $\tau_{av} \sim 52.83$ μs. The result obtained is highly suitable for the proposed security ink applications as well as many other optical display applications.

Finally, the transparent multi-stage excitable security inks application of Y_2O_3:Yb^{3+}/Er^{3+} nanorods for anti-counterfeiting applications, which was not reported earlier, was demonstrated.[25–27] The main advantages of using standard gold PVC medium for the dispersion of luminescent nanorods are its easy availability in the market at a low cost, convenience of printing, highly stability and the sticky nature of medium (viscosity ~3000 μP) with paper which is highly desirable for such applications. For the successful demonstration of anti-counterfeiting applications, first the luminescent security ink was synthesized. For this purpose, specific amount of luminescent nanorods was incorporated in PVC gold medium. The ratio of luminescent nanorod powder and PVC gold medium has been described in detail in the experimental section. In order to examine the dispersion of Y_2O_3:Yb^{3+}/Er^{3+} nanorods in PVC gold medium, the transparent security ink solution was excited by a 980 nm wavelength diode laser which can be tuned to a maximum of 0–6 W, as shown in Fig. S14 (see ESI†). An SEM image of the sample upon its dispersion into PVC gold medium was also taken as shown in Fig. S15 (see ESI†). The synthesized ink is highly stable for several hours and also maintains its optical transparency with higher luminescence. Furthermore, for the printing of security codes, a standard screen printing technique was used. The detailed systematic process of screen printing on black paper in the present investigations is shown in Fig. 6a. The image of Mahatma Gandhi, alphabets and circular spots were printed on black paper to demonstrate the anti-counterfeiting applications. Fig. 6b demonstrates the printed pattern under different excitation wavelengths (379 and 980 nm). The pattern is printed on black paper using transparent security ink synthesized in the present investigation which can be easily seen in Fig. 6b. The visibility of the printed item is almost negligible in normal light. When the printed patterns (circular spots) were excited under a 980 nm laser light, they showed red and green coloured emissions. Furthermore, when other printed patterns (a sketched image of Mahatma Gandhi and alphabets) were exposed to an excitation wavelength of 379 nm, a green coloured emission was exhibited which can be easily seen at the right-hand side of Fig. 6b. The fluorescent mapping of the selected area of the printed luminescent alphabets was further examined to validate the distribution of the Y_2O_3:Yb^{3+}/ Er^{3+} nanorods in PVC gold medium. Fig. 6c shows the PL mapping of that particular area upon excitation by wavelengths of 375, 980 and 1550 nm as shown in Fig. 6c (i), (ii) & (iii), respectively, together with their corresponding PL spectra. The clear evidence of PL and PL mapping at various wavelengths prove its potential use for multi-stage security ink applications to prevent counterfeiting. Finally, a realistic scheme was

This journal is © The Royal Society of Chemistry 2014

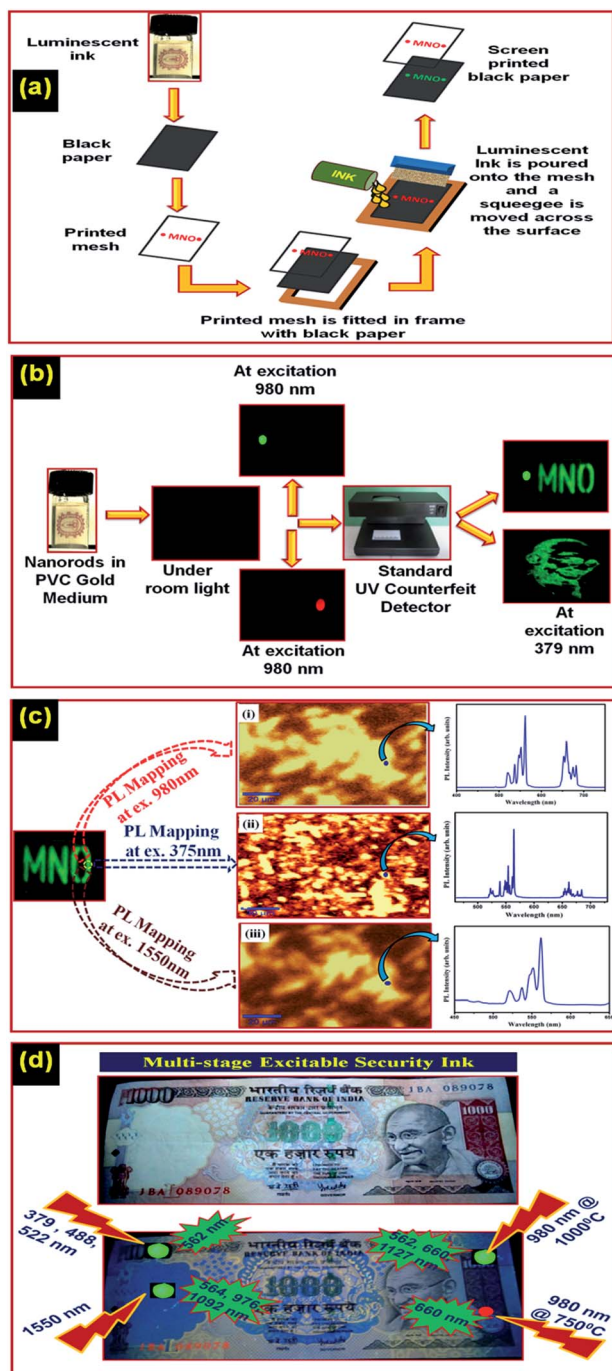*J. Mater. Chem. C*, 2014, **2**, 10468–10475 | **10473**

Fig. 6 (a) Demonstrates various steps involved in the systematic process for screen printing on black paper, (b) printed pattern images of Mahatma Gandhi and alphabets exposed to a 379 nm excitation wavelength, and it can be easily seen that these images clearly show the strong green colour emission and the images are clearly visible, (c) the PL mapping image of the selected region of printed alphabets excited with multi-stage excitation wavelengths at 375, 980 and 1550 nm as shown in (i), (ii) and (iii) and their PL spectra, respectively and (d) the proposed scheme for high-end protection of Indian currencies to protect counterfeiting.

demonstrated on the basis of the obtained spectroscopic results which is a legitimate proof of its application for high-end protection of Indian currency as shown in Fig. 6d. Concisely, the

results obtained reveal that Y_2O_3:Yb^{3+}/Er^{3+} nanorods have good structural properties, optical properties, excellent solubility in PVC gold medium and can be easily produced at a large scale for commercial printing applications. The results achieved reveal that Y_2O_3:Yb^{3+}/Er^{3+} nanorods can be the ultimate choice for a multi-stage security ink application for anti-counterfeiting. Therefore, we can expect Y_2O_3:Yb^{3+}/Er^{3+} nanorods to offer a new perspective for the fabrication of low-cost multi-stage security ink for advanced anti-counterfeiting applications.

Conclusions

In summary, the development of a novel, multi-stage excitable (379 nm, 980 nm and 1550 nm) and highly-luminescent Y_2O_3:Yb^{3+}/Er^{3+} nanorod based transparent (~81%) security ink has been successfully demonstrated. These luminescent nanorods were synthesized using a hydrothermal method which can be scaled up in large quantity and it could emit both hyper-sensitive green and strong red in a single host lattice at different excitation wavelengths. Furthermore, these nanorods have exhibited both down-shift as well as up-conversion features at a single excitation NIR wavelength of 980 nm. Furthermore, these luminescent nanorods have exhibited the striking features related to the tuning of emission colours from red to green by controlling the sintering temperature. Thus, the integration of luminescent nanorods with a suitable PVC gold medium offers new opportunities for high-end multi-stage excitable transparent security ink which is highly useful for protection against counterfeiting of important documents as well as for currency.

Acknowledgements

Notes and references

1 B. L. Volodin, B. Kippelen, K. Meerholz, B. Javidi and N. Peyghambarian, *Nature*, 1996, **83**, 58–60.

2 B. K. Gupta, D. Haranath, S. Saini, V. N. Singh and V. Shanker, *Nanotechnology*, 2010, **21**, 055607.

3 S. Armstrong, O. Graydon, D. Pile and R. Won, *Nat. Photonics*, 2012, **6**, 801.

4 W. J. Kim, M. Nyk and P. N. Prasad, *Nanotechnology*, 2009, **20**, 185301.

5 J. M. Meruga, W. M. Cross, P. S. May, Q. Luu, G. A. Crawford and J. J. Kellar, *Nanotechnology*, 2012, **23**, 395201.

6 C. E. Chesak, *Opt. Commun.*, 1995, **115**, 429–436.

7 J. Janucki and J. Owsik, *Opt. Commun.*, 2003, **228**, 63–69.

8 A. K. Aggarwal, S. K. Kaura, D. P. Chhachhia and A. K. Sharma, *Opt. Laser Technol.*, 2006, **38**, 117–121.

10474 | *J. Mater. Chem. C*, 2014, **2**, 10468–10475

This journal is © The Royal Society of Chemistry 2014

9 B. Yoon, J. Lee, I. S. Park, S. Jeon, J. Lee and J. M. Kim, *J. Mater. Chem. C*, 2013, **1**, 2388–2403.

10 Y. Cui, R. S. Hegde, I. Y. Phang, H. K. Lee and X. Y. Ling, *Nanoscale*, 2014, **6**, 282–288.

11 K. Huang, J. M. Carulli and Y. Makris, *International Conference IEEE*, 2013.

12 A. K. Deisingh, *Analyst*, 2005, **130**, 271–279.

13 A. Mills, *Chem. Soc. Rev.*, 2005, **34**, 1003–1011.

14 R. Abargues, P. J. Rodriguez-Canto, S. Albert, I. Suarezb and P. Martínez-Pastor, *J. Mater. Chem. C*, 2014, **2**, 908–915.

15 V. K. Rai, A. Pandey and R. Dey, *J. Appl. Phys.*, 2013, **113**, 083104.

16 A. P. Singh, B. K. Gupta, M. Mishra, Govind, A. Chandra, R. B. Mathur and S. K. Dhawan, *Carbon*, 2013, **56**, 86–96.

17 A. Ubaldini and M. M. Carnasciali, *J. Alloys Compd.*, 2008, **454**, 374–378.

18 H. Guo and Y. M. Qiao, *Opt. Mater.*, 2009, **31**, 583–589.

19 B. Tang, J. Ge, C. Wu, L. Zhuo, J. Niu, Z. Chen, Z. Shi and Y. Dong, *Nanotechnology*, 2004, **15**, 1273–1276.

20 X. Li, Q. Li, J. Wang and J. Li, *J. Lumin.*, 2007, **124**, 351–356.

21 L. Yanhoung, Z. Yongming, H. Guangyan and Y. Yongning, *J. Rare Earths*, 2008, **26**, 450–454.

22 A. Martíneza, J. Moralesa, P. Salasb, C. Angeles-Chávezb, L. A. Díaz-Torresc and E. De la Rosa, *Microelectron. J.*, 2008, **39**, 551–555.

23 B. K. Gupta, N. N. Tharangattu, S. A. Vithayathil, Y. Lee, S. Koshy, A. L. M. Reddy, A. Saha, V. Shanker, V. N. Singh, B. A. Kaipparettu, A. A. Martí and P. M. Ajayan, *Small*, 2012, **8**, 3028–3034.

24 B. K. Gupta, T. Palanisamy, N. N. Tharangattu, L. Song, G. Wei, H. Takuya, A. L. M. Reddy, A. Saha, V. Shanker, M. Endo, A. A. Martí and P. M. Ajayan, *Nano Lett.*, 2011, **11**, 5227–5533.

25 Y. Liu, K. Ai and L. Lu, *Nanoscale*, 2011, **3**, 4804–4810.

26 J. Wang, T. Wei, X. Li, B. Zhang, J. Wang, C. Huang and Q. Yuan, *Angew. Chem., Int. Ed.*, 2014, **53**, 1616–1620.

27 Y. Zhang, L. Zhang, R. Deng, J. Tian, Y. Zong, D. Jin and X. Liu, *J. Am. Chem. Soc.*, 2014, **136**, 4893–4896.

This journal is © The Royal Society of Chemistry 2014

J. Mater. Chem. C, 2014, **2**, 10468–10475 | **10475**